jove

Quantifying Elastic Properties of Environmental Biofilms using Optical Coherence Elastography

Evan Dieppa[1], **Hannah Schmitz**[2], **Ziwei Wang**[3], **Fabrizio Sabba**[4], **George Wells**[2], **Oluwaseyi Balogun**[1,2,3]

[1] Theoretical and Applied Mechanics Program, Northwestern University [2] Civil and Environmental Engineering Department, Northwestern University [3] Mechanical Engineering Department, Northwestern University [4] Black & Veatch

Corresponding Author

Oluwaseyi Balogun
o-balogun@northwestern.edu

Citation

Dieppa, E., Schmitz, H., Wang, Z., Sabba, F., Wells, G., Balogun, O. Quantifying Elastic Properties of Environmental Biofilms using Optical Coherence Elastography. *J. Vis. Exp.* (205), e66118, doi:10.3791/66118 (2024).

Date Published

March 1, 2024

DOI

10.3791/66118

URL

jove.com/video/66118

Abstract

Biofilms are complex biomaterials comprising a well-organized network of microbial cells encased in self-produced extracellular polymeric substances (EPS). This paper presents a detailed account of the implementation of optical coherence elastography (OCE) measurements tailored for the elastic characterization of biofilms. OCE is a non-destructive optical technique that enables the local mapping of the microstructure, morphology, and viscoelastic properties of partially transparent soft materials with high spatial and temporal resolution. We provide a comprehensive guide detailing the essential procedures for the correct implementation of this technique, along with a methodology to estimate the bulk Young's modulus of granular biofilms from the collected measurements. These consist of the system setup, data acquisition, and postprocessing. In the discussion, we delve into the underlying physics of the sensors used in OCE and explore the fundamental limitations regarding the spatial and temporal scales of OCE measurements. We conclude with potential future directions for advancing the OCE technique to facilitate elastic measurements of environmental biofilms.

Introduction

In wastewater treatment and water resource recovery, beneficial biofilms in attached growth reactors are increasingly employed to enable microbes to convert undesirable pollutants, such as organic matter, nitrogen, and phosphate, into stabilized forms that can be easily removed from the water[1]. In these systems, the biofilm's emergent function, namely biochemical transformations, is closely associated with the diversity of microbes residing in it and the nutrients these microbes receive[2]. Accordingly, ongoing biofilm growth can pose a challenge to maintaining consistent reactor functionality because the new biofilm growth may alter the biofilm's overall metabolic processes, mass transfer characteristics, and community composition. Stabilizing the biofilm environment as much as possible can protect against such changes[3]. This includes ensuring a consistent flow of nutrients and keeping the structure of the biofilm stable with

a steady thickness[4]. Monitoring the biofilm's stiffness and physical structure would enable researchers to gain insight into the overall health and functioning of the biofilm.

Biofilms exhibit viscoelastic properties[5,6,7]. This viscoelastic nature results in a combination of an instantaneous and slow, time-dependent deformation in response to external mechanical forces. One unique aspect of biofilms is that, when they are subjected to substantial deformation, they respond like viscous liquids. Conversely, when subjected to minor deformation, their response is comparable to solids[5]. Moreover, within this small-deformation region, there is a deformation range under which biofilms exhibit a linear force-displacement relationship[5,6,7]. Deformations within this linear range are optimal for assessing biofilm mechanical characteristics because these yield reproducible measurements. Several techniques can quantify the elastic response within this range. Optical coherence elastography (OCE) is an emerging technique that is being adapted for analyzing biofilms in this linear range (strains on the order of 10^{-4}-10^{-5})[8,9].

OCE's most established application so far is in the biomedical field, where the technique has been applied to characterize biological tissues that only require superficial optical access. For example, Li et al. used OCE to characterize the elastic properties of skin tissue[10]. Other authors characterized the anisotropic elastic properties of porcine and human corneal tissues and how they are affected by intraocular pressure[11,12,13,14,15,16]. Some advantages of the OCE method for studying biofilms are that it is non-destructive and provides mesoscale spatial resolution, it does not require any sample preparation, and the method itself is rapid; it provides co-registered measurements of physical structure and elastic properties (e.g., porosity, surface roughness, and morphology)[8,9,17,18].

The OCE method measures the local displacement of propagating elastic waves in a specimen using phase-sensitive optical coherence tomography (OCT). OCT is a low-coherence optical interferometer that transforms local changes in the sample displacement into an intensity change that is recorded with an optical spectrometer. The OCT technique has also been utilized in biofilm research for the characterization of mesoscale structure, porosity distribution in three dimensions, and biofilm deformation[17,19,20,21]. In addition, Picioreanu et al. estimated biofilm mechanical properties using fluid-structure interaction inverse modeling of OCT cross-sectional deformation images[22].

On the other hand, OCE measurements, coupled with inverse elastodynamic wave modeling, yield the wave speed of elastic waves in the sample, which enables the characterization of the elastic and viscoelastic properties of the sample. Our group adapted the OCE technique for quantitative measurement of biofilm elastic and viscoelastic properties[8,9,18] and validated the technique against shear rheometry measurements in agarose gel plate samples[18]. The OCE approach provides precise and reliable estimates of the biofilm properties since the measured elastic wave speed is correlated with the elastic properties of the sample. Furthermore, the spatial decay of the elastic wave amplitude can be directly correlated with the viscoelastic properties due to viscous effects in the material. We have reported OCE measurements of viscoelastic properties of mixed culture bacterial biofilms grown on coupons in a rotating annular reactor (RAR) and granular biofilms with complex geometries using elastodynamic wave models[18].

The OCE technique is also a powerful alternative to traditional rheometry[18] which is used for viscoelastic characterization. Rheometry methods are best suited for samples with planar geometry. As such, granular biofilms, which have arbitrary shapes and surface morphologies, cannot be accurately characterized on a rheometer[8,23]. In addition, unlike OCE, rheometry methods may be challenging to adapt for real-time measurements, for example, during biofilm growth in flow cells[24,25].

In this paper, we show that OCE measurements of the frequency-independent wave speed of surface waves can be used to characterize the biofilm elastic properties without the need for complicated models. This development will make the OCE approach more accessible to the broader biofilm community for studying the biofilm mechanical properties.

Figure 1 shows a schematic illustration of the OCT system used in this study. The system incorporates several instruments, including a commercial spectral-domain phase-sensitive OCT system, a delay generator, a function generator, and a piezoelectric transducer. The OCT system operates on the principle of interferometry by employing a broadband light source with a center wavelength of 930 nm. The collected light intensity, which is correlated with intricate structural details in the sample, is analyzed in the postprocessing unit and then converted to a cross-sectional image of the sample - commonly referred to as an OCT image. The OCT imaging depth depends on the severity of the optical scattering in the sample that stems from local variation in the refractive index and is limited to 1- 3 mm in biological tissues and biofilms. Since the optical phase in the sample and the interference intensity are modulated by motion, the OCT can be used to detect the local sample displacement. We leverage the displacement sensitivity of the OCT in the OCE method to track the steady state displacement field of elastic waves in the sample. Specifically, the function generator outputs a sinusoidal voltage to drive the piezoelectric transducer. The transducer, in turn, stretches and contracts with an oscillatory time history. The oscillatory displacement of the transducer imparts a sinusoidal force on the sample surface through a 3D-printed wedge tip at the apex of the transducer, leading to the generation of harmonic elastic waves in the sample. The wedge tip makes light contact with the sample, such that the sample remains intact after the actuator is retracted from the sample surface. To record the local displacement in the sample, adjacent depth scans separated by a fixed time delay are acquired at each pixel in the sample. The optical phase difference between consecutive scans at each pixel point is proportional to the local vertical displacement at the same point. Synchronization between the displacement of the transducer and the scanning optics in the OCT system is achieved through a trigger pulse that originates from the function generator and is delayed in the delay generator. This synchronization step facilitates the acquisition of consistent cross-sectional images of the local optical phase distribution in the sample. These images are directly proportional to the local vertical harmonic displacement in the sample and are known as the OCE image. OCE images are acquired at different transducer actuation frequencies to obtain the elastic wavelength and wave speed as a function of frequency. The wave speeds measured are analyzed with an elastodynamic model to determine the elastic properties of the sample.

Protocol

1. System setup

1. Gather the system components which include the commercial OCT system (base unit, stand, imaging

head, and computer), waveform generator, transducer, delay/pulse generator, a switch with BNC connections, BNC cables and adapters, optical posts, and clamps.

2. Connect the sync signal from the function generator to a switch. Connect the other port of the switch to the delay generator.
3. Connect the output of the function generator to the transducer leads.
4. Connect the outputs of the delay generator to the trigger channel at the back of the OCT base unit. The output signal from the delay generator is a trigger pulse to initiate the motion of the scanning optics in the OCT system.
5. Turn on the system components (OCT base unit, computer, function generator, and delay generator) and launch the OCT software.
6. Configure the delay generator to send a transistor-transistor logic trigger signal to the OCT base unit. Refer to the OCT system manual for the trigger signal requirements.
7. Position the transducer beneath the OCT lens. The transducer has a 3D-printed wedge tip glued onto one of its ends that serves as a line source for elastic waves.

2. Image acquisition

1. On the OCT software, select the **Doppler Acquisition Mode** and enable the external trigger.
2. Place the granular biofilm under the lens in a sample holder and move it towards the tip of the transducer using a translation stage. Ensure that the transducer makes gentle contact with the sample surface, as shown in **Figure 2**. We used two granular biofilms (also known as granular sludge) with different nominal diameters (4.3 mm and 3.3 mm). This selection was made to investigate the impact of biofilm size on its mechanical properties. These were commercially obtained.

   NOTE: The sample holder employed in this study consists of a 3D-printed plastic plate with multiple hemispherical indentations. This holder does not allow for measurements under native conditions. Therefore, we introduced water from the natural environment during measurements to prevent the sample from drying.
3. Specify the scan region by clicking the **Start and Endpoints of the Line of Interest** (wave propagation path) in the sample monitor window. Center this line with respect to the transducer tip and ensure it is perpendicular to the edge of the tip.
4. Specify the number of pixels along the scan region and the depth of the sample and increase the number of B-scans (2D cross-sectional images) to be recorded to improve the signal-to-noise ratio of the OCE images. The presented results were obtained using 1523 pixels along the scanning path and 1024 pixels along the depth. A total of 50 B-scans were taken.
5. Click the **Scan** button and turn ON the switch. The OCT and OCE images should appear on the screen. Activate the switch within the trigger timeout time and the scan preparation time.
6. Ensure that the reference intensity is within the optimum range and position the sample within the focal region of the OCT microscope objective. A properly focused sample should have its top edge close to the top of the image.
7. Adjust the phase contour in the OCE image on the display toolbar by increasing the higher value of the left-hand side color bar and decreasing the lower value of the right-hand side color bar. This will increase the fringe contrast.

8. Configure the function generator to produce a single-frequency sinusoidal voltage by pressing the **Sine** button in the front panel and specify the starting excitation frequency for the measurements. The measurements in this study start at 4 kHz and end at 9.6 kHz. Enable the Output connector by pressing the Output key.
9. Set an acceptable voltage for the measurement. This value should maximize fringe visibility but also avoid phase wrapping. For the biofilms in this study and the frequency range of the measurements, a voltage between 5 and 10 V typically results in a phase map with good contrast.
10. Acquire the OCT and OCE images by clicking the **Record** button.
11. Repeat the measurements at different frequencies to obtain cross-sectional images of the elastic wave field with different wavelengths (or fringe periods).

3. Image Analysis

1. Obtain the physical size of the pixels. The physical pixel size in x is obtained by dividing the field of view in the x direction by the image size in the x direction and then multiplying by a factor of two. The physical pixel size in z is obtained by dividing the field of view in the z direction by the image size in the z direction. The field of view and image size values are stored in the structure array with the image information which can be accessed with the OCTFileOpen function provided in the MATLAB SDK in the ThorImageOCT package.
2. Obtain the OCT and OCE matrices using the OCTFileGetIntensity and OCTFileGetPhase functions, respectively, and take the average of the recorded frames. These functions are provided in the MATLAB SDK in the ThorImageOCT package.
3. Obtain the pixel locations of the top edge of the sample by binarizing the image and detecting the white pixels from top to bottom for each column.
4. Extract the phase distribution of the OCE image along this edge using the improfile function and compute the cumulative arc length in real dimensions. Compute the arc length by taking the cumulative sum of the norm of scaled differences between consecutive points in the x and z directions.
5. Compute the spatial fast Fourier transform of the measured OCT phase distribution (i.e., from the OCE images) with respect to the cumulative arc length using the plomb function.
6. Determine the location of the peak in the spectrum. This location represents the spatial frequency of the wave. Calculate the wave speed (or phase velocity) from the ratio of the transducer excitation frequency (units of Hz) and the spatial frequency (unit of inverse length).

Representative Results

In this study, we used granular biofilms (also known as granular sludge), which were commercially obtained. Granules are spherical biofilms that form through self-aggregation, meaning that they do not require a carrier or surface on which to grow[26]. **Figure 3A** shows a representative cross-sectional OCT image that arises due to the spatial variation of the local refractive index in a granular biofilm. The biofilm has a nominal diameter of 3 mm. Some of the internal features, including pores and voids that are close to the sample's surface, are seen in the image. Increased optical scattering along the sample's depth prevents the

OCT light source from reaching the center of the sample, thus rendering the central region devoid of any discernible information. **Figure 3B** shows the cross-sectional OCE image of the sample for a transducer excitation frequency of 5.1 kHz. The local contrast in the image is correlated with the local vertical displacement induced by the propagating elastic wave in the sample. The physical spacing of the fringes along the propagation path corresponds to the wavelength of the elastic surface wave. The surface wave propagates near the sample surface, and it has a penetration depth that is close to the wavelength. The spatial extent of the surface wave displacement is not seen in the image due to the limited optical penetration of the OCT light source in the sample. The optical phase distribution along the elastic wave propagation path (**Figure 4A**) is used to determine the spatial frequency of the surface wave. The spatial frequency is obtained by taking the fast Fourier Transform (FFT; **Figure 4B**) of the data and selecting the frequency at which the magnitude of the FFT spectrum is largest.

It is crucial to select a function generator voltage of sufficient magnitude to produce a fringe pattern that exhibits optimal contrast in the OCE image. However, excessively large voltages should be avoided as this can result in phase wrapping in the OCE image, as illustrated in **Figure 5A**. Phase wrapping arises because the optical phase difference in the measurement is restricted to the interval between -π and π. When the phase exceeds one of these limits, it is folded to the opposite limit, creating a discontinuous phase distribution. Consequently, the need for phase unwrapping arises, which poses challenges and can introduce potential inaccuracies. Another factor to consider for accurate wave measurements is the number of fringes present within the OCE image. At low transducer frequencies, depicted in **Figure 5B**, a complete oscillation cycle of the surface wave may not be fully captured due to the small size of the granule, and the FFT spectrum may yield erroneous estimates for the spatial frequency (or inverse wavelength). Another source of error in the spatial frequency estimate is the presence of spatially overlapping elastic wave modes, such as surface waves and bulk shear waves, in the OCT image. These wave modes mix, setting up complicated interference patterns that may be difficult to analyze. The presence of various wave modes beyond surface waves can introduce interference effects near the transducer, contingent upon the specific sample, excitation frequency, and amplitude. **Figure 6** is an example of an OCE image obtained with an excitation frequency of 5.5 kHz, in which a bulk shear wave near the local excitation point interferes with the surface wave field. **Figure 7A** portrays a phase distribution that diverges from the decaying sine wave pattern observed in **Figure 4A**, attributed to the combination of wave modes. Consequently, the resultant FFT exhibits a broader peak, as depicted in **Figure 7B**. The same phenomenon can occur close to defects like voids or regions with marked variations in elastic/viscoelastic properties. In these areas, the local displacement field is modified due to interference of the incident or surface wave and the scattered waves from the defect.

We calculated the wave speed for the surface wave at frequencies between 4.0 and 9.6 kHz for two granular biofilms with different nominal diameters (4.3 mm and 3.3 mm). The wave speed plots are called dispersion curves. For the settings used, each dispersion measurement took approximately 15 min. Within the selected frequency interval, multiple cycles of the sinusoidal displacement profile are present in the OCE images, enabling precise determination of spatial frequency alongside notable phase contrast. **Figure 8** illustrates the obtained dispersion curves. These curves represent the average dispersion curves for three locations

within each sample. The surface wave speeds approach a constant value, called the Rayleigh wave speed, c_R, which is related to the shear modulus of the sample through the relation,

$$c_R = ((0.862 + 1.14\nu)/ (1 + \nu)) \times (G/r)^{1/2}$$

where, G is the shear modulus, r is the mass density, and ν is the Poisson's ratio[27,28]. It is constant because the penetration depth of the elastic wave is shorter than the diameter of the sample. Essentially, the elastic wave travels close to the surface of the sample with a wave speed that is directly proportional to the square of the Young's modulus[28]. However, due to measurement noise, the wave speed is not entirely constant in this frequency range. We take the average of the wave speeds for frequencies between 6.0 and 9.6 kHz for the smaller sample and between 4.0 and 9.6 kHz for the larger sample. This average wave speed is then employed for estimating the Young's modulus of the sample.

We assume that the sample is incompressible due to its high-water content. As such, **v** = 0.5. Thus, c_R is directly related to E = 3G for an incompressible solid, where E is the Young's modulus of the sample[27,28]. The dashed lines in **Figure 8** represent the Rayleigh wave speeds for the different samples. We assume a biofilm composition primarily comprising water, yielding a density of 1000 kg/ m^3. Consequently, the calculated Young's modulus of the granular biofilms is 85 kPa and 205 kPa for the granular biofilms with nominal diameters of 4.3 mm and 3.3 mm, respectively. This measurement confirms the technique's capability to discern mechanical property differences among the biofilms.

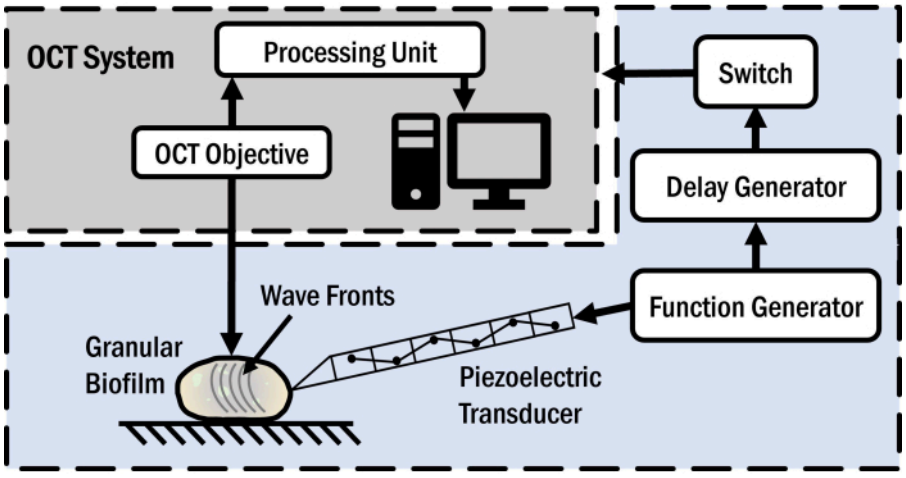

Figure 1: Optical coherence elastography setup. The schematic of the system used here is shown in the figure. Please click here to view a larger version of this figure.

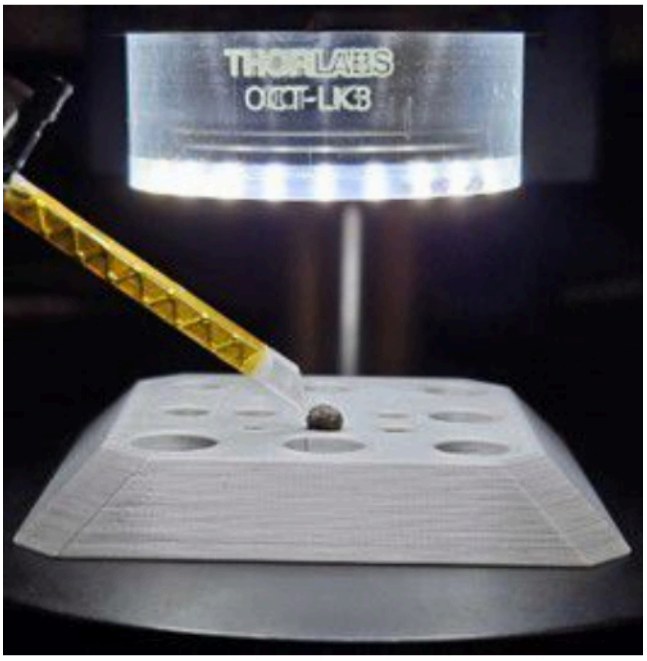

Figure 2: Mounted sample. The granular biofilm is positioned on the sample holder while the transducer makes gentle contact with it. Please click here to view a larger version of this figure.

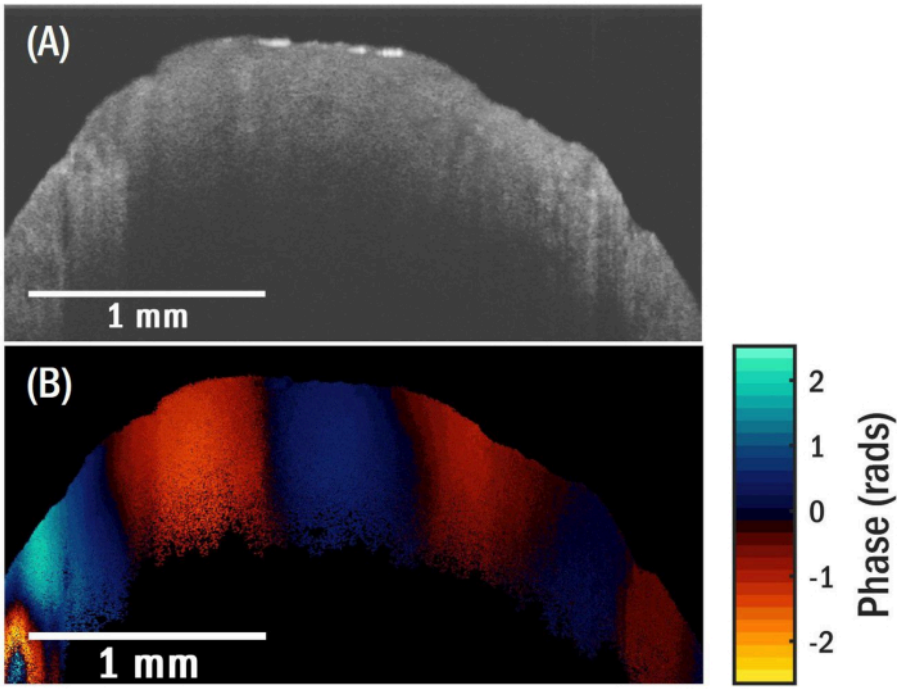

Figure 3: OCT and OCT images of granular biofilm. (**A**) OCT image. (**B**) OCE image for a surface wave propagating at 5.1 kHz showing good fringe contrast. Please click here to view a larger version of this figure.

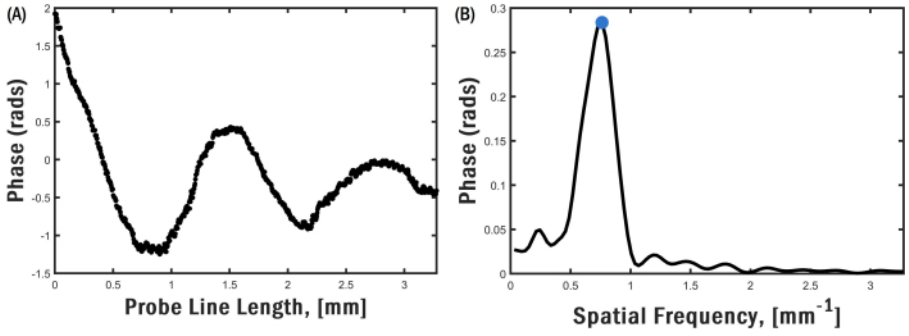

Figure 4: Phase distribution and FFT. For the image shown in **Figure 3B**, (**A**) phase difference distribution along the top edge of the sample and (**B**) FFT of the phase difference distribution showing a narrow peak. Please click here to view a larger version of this figure.

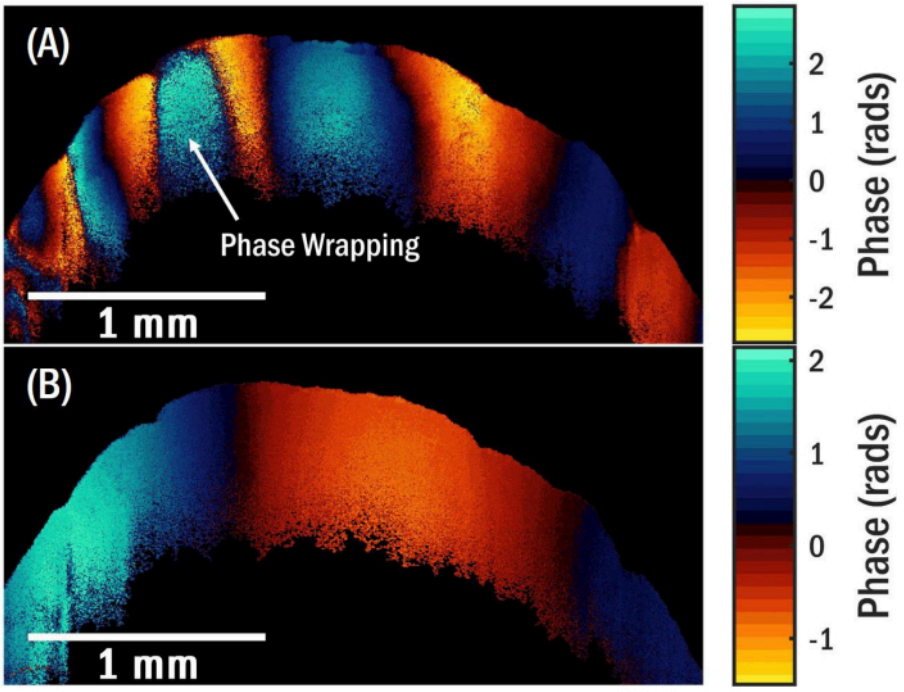

Figure 5: OCT and OCT images of granular biofilm. (**A**) OCE image for a surface wave propagating at 5.1 kHz showing phase wrapping. (**B**) OCE image for a surface wave propagating at 1.3 kHz without a complete cycle. Please click here to view a larger version of this figure.

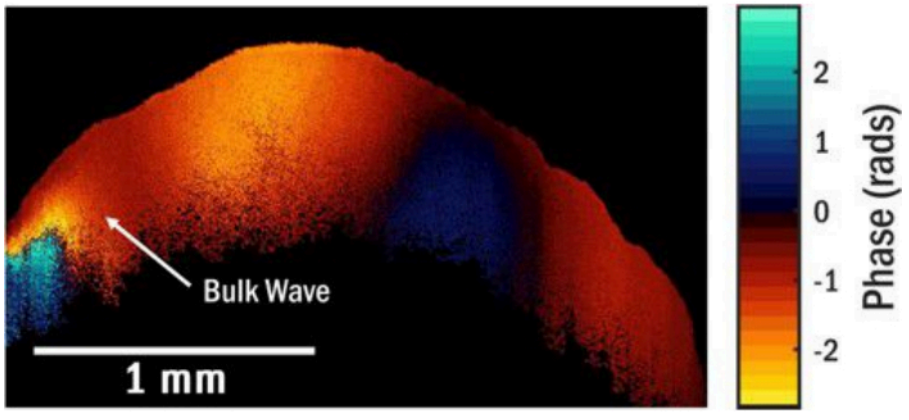

Figure 6: OCE image showing a combination of modes. This image is from a different location of the sample and illustrates the combination of modes for a wave propagating at 5.5 kHz. Please click here to view a larger version of this figure.

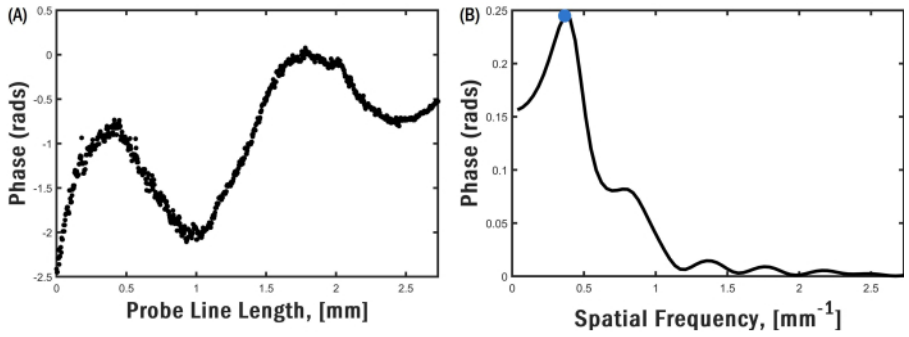

Figure 7: Phase distribution and FFT. For the image shown in **Figure 6,** (**A**) phase difference distribution along the top edge of the sample and (**B**) FFT of the phase difference distribution showing a broader peak. Please click here to view a larger version of this figure.

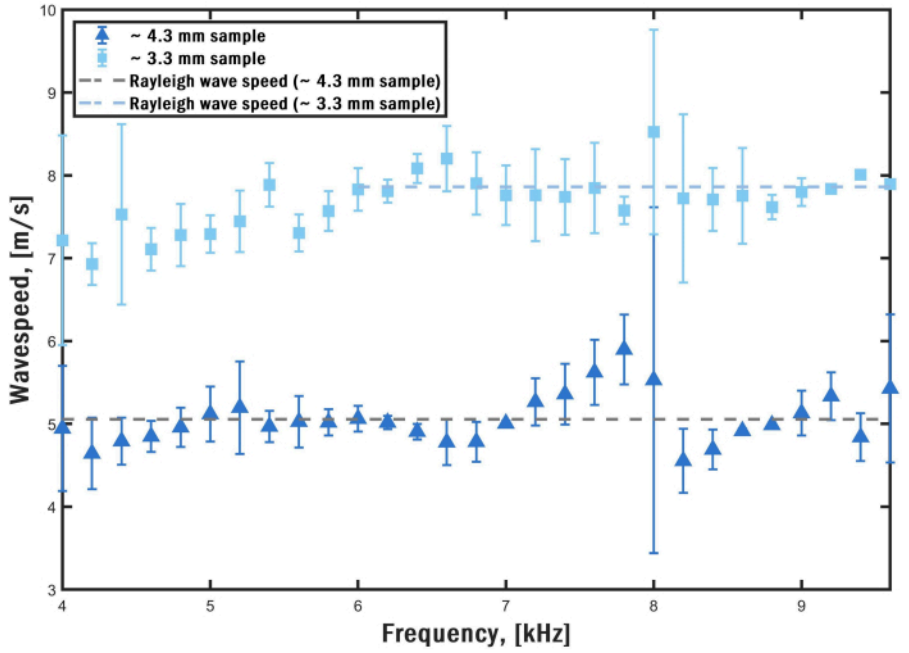

Figure 8: Dispersion curves. The wave speed in two samples with different sizes is shown at different frequencies with standard deviation bars. The corresponding Rayleigh wave speed for the flat portion of the curves is plotted on top. Please click here to view a larger version of this figure.

Discussion

The attainable imaging depth in the OCT system is determined by the degree of light penetration from the light source, which depends on the wavelength of the source. Moreover, the wavelength determines the axial resolution. Longer wavelengths can penetrate more deeply into the sample but at the expense of reduced axial resolution compared to shorter wavelengths. Transverse resolution, on the other hand, is dependent on both the numerical aperture of the system and the wavelength, with shorter wavelengths delivering higher resolution. Increasing the numerical aperture introduces a trade-off by limiting the depth of field[29]. The spatial resolution is limited to the shortest elastic wavelength that can be detected with a sufficient signal-to-noise ratio. The current OCE methodology is limited to 0.5 mm[9,30]. While this technique is limited by the size of the sample, it should be applicable to various biofilm types. The shape of the biofilm, granular or flat, will not inhibit the technique. The transparency of the sample also plays a role in determining penetration depth. Materials with high transparency enable light to pass through all the sample, rendering it imperceptible to observation, whereas opaque samples impede light penetration, yielding minimal details about their internal structure[9,28]. In the context of this study, a penetration depth in the millimeter range suffices.

Another possible issue for these measurements is that in larger samples, in which the size does not limit the number of elastic wave cycles, the field-of-view (FOV) of the OCT microscope may be the limiting factor of the number of measured cycles. For measurements here, the FOV is limited to 9 mm by 9 mm; thus, elastic wavelengths longer than 9 mm cannot be resolved in this OCT microscope. Utilizing a lens with a broader field of view would enable the imaging of larger samples, yielding more fringes at these lower frequencies. Challenges arise at higher frequencies as well. For the samples in this study, beyond 10 kHz, the wave experiences significant attenuation, diminishing the magnitude of the phase difference distribution and complicating the determination of the spatial frequency. This concern can be mitigated by augmenting the voltage of the function generator, thereby increasing the transducer's displacement. However, increasing the displacement is just useful up to a certain point as this will eventually end up in phase wrapping[9]. Alternatively, enhancing the system's sensitivity by implementing a light source with higher power can counteract phase wrapping caused by larger displacements and facilitate the detection of the dynamic response to smaller excitations. A higher sensitivity facilitates the implementation of acoustic OCE methods that offer the benefit of non-contact loading but are more profoundly affected by the high attenuation[31].

When conducting these measurements on biofilms, it is crucial to keep the samples hydrated. Drying leads to an undesirable increase in stiffness, which is irrelevant since the focus is on assessing the sample's properties under its native environment. We did not study illumination-induced drying. However, we remark that water from the natural environment was added periodically throughout the measurement, and during that time, the sample morphology was monitored through the OCT images, and no discernible changes in the morphology were observed. Additionally, when positioning the transducer and capturing OCE images, it's essential to account for the features discerned in the OCT image. Heterogeneities along the wave propagation path have the potential to distort the wave field and should thus be avoided[9]. Furthermore, maintaining gentle contact with the biofilm is crucial, as excessive pressure on the sample, aside from potentially modifying its mechanical characteristics, could

also lead to distortion of the wave field. Finally, the scan region must be perpendicular to the wavefronts to ensure that the spatial frequency of the harmonic wave is accurately determined from the measurement.

For some frequencies, significant variations in wave speeds were observed in both samples, which can be ascribed to their inherent heterogeneities, wavefield at that specific frequency, and morphology of the propagation paths. We previously showed that the measured wave speed profile across a sectioned granular biofilm is non-uniform due to the heterogeneous microstructure[9]. Consequently, when employing this technique on granular biofilms, it is imperative to conduct measurements at multiple locations across the sample to derive an averaged representation.

An important observation regarding the dispersion curves is that they exhibit distinct behaviors for different sample sizes. In the case of the larger sample, the curve remains relatively constant across the measured range. However, for the smaller sample, there is an upward trend in wave speed with increasing frequency, particularly in the lower portion of the range. This phenomenon can be ascribed to the presence of viscoelastic effects at lower frequencies and the generation of elastic waveguide modes. We accounted for these effects in our previous work using more sophisticated inverse models[8,9,18].

It is important to note that in aerobic granular systems, biomass is not evenly distributed throughout the height of the reactor. During non-aeration phases, larger granules tend to settle at the bottom of the reactor. This uneven distribution results in aggregates of different sizes having access to varying amounts of substrate. As a result, aggregates of different sizes exhibit distinct community composition. Additionally, because excess sludge is selectively removed, larger granules tend to be retained in the reactor for longer periods, while smaller ones are more easily removed[32]. The noticeable difference in Young's modulus suggests a potential connection between biofilm composition, age, and mechanical properties.

In summary, the Optical Coherence Elastography (OCE) method offers a rapid and non-destructive means of assessing elastic wave speed in biofilms. This method overcomes the constraints of rheological measurements and exhibits enhanced attributes in comparison to alternative elastography techniques[8,18]. Moreover, its applicability extends beyond granular biofilms to encompass any partially transparent sample with suitable optical penetration depth and size large enough to be resolved by the system, including examples like hydrogels[33], cornea[34], and skin[35]. The method's future advancements encompass several key aspects. Firstly, increasing the frequency of harmonic elastic waves into the hundreds of kHz range will allow for wavelengths of a few micrometers, thereby achieving spatial resolution at a similar scale. Secondly, the signal-to-noise ratio of the optical detection system will be enhanced by increasing the optical power of the OCT system from 2 mW (current) to 20 mW. Lastly, we will replace the contact harmonic actuator with a non-contact acoustic radiation pressure source. This addition will facilitate non-invasive and non-destructive operation and allow for interrogating biofilm samples in their native environments.

Disclosures

The authors declare no conflicts of interest.

Acknowledgments

The authors thank Aqua-Aerobic Systems, Inc. (Rockford, IL, USA) for providing the granular biofilms studied in this

work. The authors also acknowledge the National Science Foundation's support via Award #210047 and #193729.

References

1. Mahto, K. U., Das, S. Bacterial biofilm and extracellular polymeric substances in the moving bed biofilm reactor for wastewater treatment: A review. *Bioresour Technol.* **345**, 126476 (2022).
2. Pholchan, M. K., Baptista, J. de C., Davenport, R. J., Curtis, T. P. Systematic study of the effect of operating variables on reactor performance and microbial diversity in laboratory-scale activated sludge reactors. *Water Res.* **44** (5), 1341-1352 (2010).
3. Briones, A., Raskin, L. Diversity and dynamics of microbial communities in engineered environments and their implications for process stability. *Curr Opin Biotechnol.* **14** (3), 270 - 276 (2003).
4. Sanchez-Huerta, C., Sanchez Medina, J., Wang, C., Fortunato, L., Hong, P. Understanding the role of sorption and biodegradation in the removal of organic micropollutants by membrane aerated biofilm reactor (MABR) with different biofilm thickness. *Water Res.* **236,** 119935 (2023).
5. Wang, H. F., Hu, H., Yang, H.Y., Zeng, R. J. Characterization of anaerobic granular sludge using a rheological approach. *Water Res.* **106**, 116-125 (2016).
6. Ma, Y. J., Xia, C. W., Yang, H. Y., Zeng, R. J. A rheological approach to analyze aerobic granular sludge. *Water Res.* **50**, 171-178 (2014).
7. Lin, X., Wang, Y. Microstructure of anammox granules and mechanisms endowing their intensity revealed by microscopic inspection and rheometry. *Water Res.* **120**, 22-31 (2017).
8. Liou, H. C. et al. Towards mechanical characterization of granular biofilms by optical coherence elastography measurements of circumferential elastic waves. *Soft Matter.* **15** (28), 5562-5573 (2019).
9. Liou H. C, Sabba F., Wang Z., Wells G., Balogun O. Layered viscoelastic properties of granular biofilms. *Water Res.* **202**, 117394 (2021).
10. Li, C., Guan, G., Reif, R., Huang, Z., Wang, R. K. Determining elastic properties of skin by measuring surface waves from an impulse mechanical stimulus using phase-sensitive optical coherence tomography. *J R Soc Interface.* **9**, 831-841 (2012).
11. Ramier, A. et al. *In vivo* measurement of shear modulus of the human cornea using optical coherence elastography. *Sci Rep.* **10**, 17366 (2020).
12. Ramier, A., Tavakol, B., Yin, S. H. Measuring mechanical wave speed, dispersion, and viscoelastic modulus of cornea using optical coherence elastography. *Optics Express.* **27** (12), 16635 (2019).
13. Crespo, M. A. et al. *In vivo* determination of human corneal elastic modulus using vibrational optical coherence tomography. *Cornea Ext Dis.* **11** (7), 1-11 (2022).
14. Ambrozinski, L. et al. Acoustic micro-tapping for non-contact 4D imaging of tissue elasticity. *Sci Rep.* **6** (38967), 1-11 (2016).
15. Pitre Jr, J. J. et al. Nearly-incompressible transverse isotropy (NITI) of cornea elasticity: model and experiments with acoustic micro-tapping OCE. *Sci Rep.* **10** (12983), 1-14 (2020).

16. Lan, G., Aglyamov, S. R., Larin, K. V., Twa, M.D. *In vivo* human corneal shear wave optical coherence elastography. *Optom Vis Sci.* **98,** 58-63 (2021).

17. Rosenthal, A. et al. Morphological analysis of pore size and connectivity in a thick mixed-cultured biofilm. *Biotechnol Bioeng.* **115**, 2268-2279 (2018).

18. Liou, H. C., Sabba, F., I. Packman, A., Wells, G., Balogun, O. Nondestructive characterization of soft materials and biofilms by measurement of guided elastic wave propagation using optical coherence elastography. *Soft Matter.* **15**, 575-586 (2019).

19. Wagner, M., Taherzadeh, D., Haisch, C., Horn, H. Investigation of the mesoscale structure and volumetric features of biofilms using optical coherence tomography. *Biotechnol Bioeng.* **107** (5), 844-853 (2010).

20. Leite-Andrade, M. C. et al. A new approach by optical coherence tomography for elucidating biofilm formation by emergent *Candida* species. *PLoS ONE.* **12** (11), e0188020 (2017).

21. Blauert, F., Horn, H., Wagner, M. Time-resolved biofilm deformation measurements using optical coherence tomography. *Biotechnol Bioeng.* **112** (9), 1893-1905 (2015).

22. Picioreanu, C., Blauert, F., Horn, H., Wagner, M. Determination of mechanical properties of biofilms by modeling the deformation measured using optical coherence tomography. *Water Res.* **145**, 588-598 (2018).

23. Li, M., Nahum, Y., Matouš, K., Stoodley, P., Nerenberg, R. Effects of biofilm heterogeneity on the apparent mechanical properties obtained by shear rheometry. *Biotechnol Bioeng.* **120**, 553-561 (2023).

24. Karimi, A., Karig, D., Kumar, A., Ardekani, A.M. Interplay of physical mechanisms and biofilm processes: review of microfluidic methods. *Lab Chip.* **15** (1), 23-42 (2015).

25. Geisel, S., Secchi, E., Vermant, J. Experimental challenges in determining the rheological properties of bacterial biofilms. *Interface Focus.* **12** (6), 20220032 (2022).

26. Winkler, M. K. H., van Loosdrecht, M. C. M. Intensifying existing urban wastewater. *Science.* **375** (6579), 377-378 (2022).

27. Graff, K. F. Wave motion in elastic solids. *Dover Publications.* (1991).

28. Kennedy, B. F., Kennedy, K. M., Sampson, D. D. A review of optical coherence elastography: Fundamentals, techniques and prospects. *IEEE J. Sel. Top. Quantum Electron.* **20** (2), 272-288 (2014).

29. Ang, M. et al. Anterior segment optical coherence tomography. *Prog Retin Eye Res.* **66**, 132-156 (2018).

30. Kirby, M. A. et al. Spatial resolution in dynamic optical coherence elastography. *J Biomed Opt.* **24** (9), 1-16 (2019).

31. Larin, K. V., Sampson, D. D. Optical coherence elastography - OCT at work in tissue biomechanics. *Biomed Opt Express.* **8**, 1172-1202 (2017).

32. Muhammad, A. et al. Importance of species sorting and immigration on the bacterial assembly of different-sized aggregates in a full-scale aerobic granular sludge. *Environ Sci Technol.* **53** (14), 8291-8301 (2019).

33. Candry, P. et al. Tailoring polyvinyl alcohol-sodium alginate (PVA-SA) hydrogel beads by controlling crosslinking pH and time. *Sci Rep.* **12** (1), 20822 (2022).

34. Kirby, M. A. et al. Optical coherence elastography in ophthalmology. *J Biomed Opt.* **22** (12), 1-28 (2017).

35. Liang, X., Boppart, S. A. Biomechanical properties of *in vivo* human skin from dynamic optical coherence elastography. *IEEE Trans Biomed Eng.* **57** (4), 953-959 (2010).